

# Communications

## Formation of Hollow Helicoids in Mesoporous Silica: Supramolecular Origami\*\*

By San Ming Yang, Igor Sokolov, Neil Coombs, Charles T. Kresge, and Geoffrey A. Ozin\*

In the past, helical shapes in nature have inspired inventions such as the water screw for agriculture, the retaining screw for wine presses, and architectural designs for spiral staircases.<sup>[1]</sup> Similarly, these days helix-shaped DNA, proteins and carbon nanotubes evoke great interest in biotechnology and nanotechnology.<sup>[2–4]</sup> Also biomimetic synthesis of helical morphologies of calcium carbonate, barium sulfate, and silica provides insight into morphogenesis of mineralized spiral forms in biology and ideas for new opportunities in materials science.<sup>[5–9]</sup> Herein we describe the synthesis of hollow helicoids made of hexagonal mesoporous silica, a remarkable topology in the materials world. They have a hierarchical architecture comprised of 5 nm diameter channels that coil in the form of a micrometer-scale tubular spiral. A population analysis of helicoid shapes defines a surprisingly narrow distribution of pitch and flute widths, pitch angles, inside and outside diameters, and significantly an equal number of left- and right-handed forms. Evidence is presented that morphogenesis involves polymerization-induced differential contraction of a patch of hexagonal silicate liquid-crystal film formed at the air–water interface, which can fold into a hollow helicoid. A supramolecular Origami theoretical model explains the creation and observed narrow distribution of mesoporous silica, hollow helicoid shapes.

Mesoporous silica hollow helicoids were prepared by using cetyltrimethylammonium chloride (CTACl) as the surfactant micellar template and tetraethylorthosilicate (TEOS) as the silica precursor. An aqueous solution of CTACl, hydrochloric acid and formamide was aged for 48 h before adding TEOS, and the material was formed

after 3 days in a quiescent state. The use of formamide in the synthesis is intentional because upon acid hydrolysis it yields ammonium chloride and formic acid to give an ultimate solution ca. pH 1.9 and an ionic strength that favors hollow helicoid formation. This solution pH is notably higher than the one used in the synthesis of mesoporous silica curved shapes.<sup>[10]</sup> Control experiments demonstrate that a high concentration of ammonium and formate ions is essential for the formation of mesoporous silica at a pH close to two, which borders on the isoelectric point of aqueous silica. We believe that a low acidity and high ionic strength medium favor a slow rate of silicification, and hence polymerization-induced differential contraction of silicate micelle rods in a patch of silicate liquid-crystal film formed at the air–water interface becomes influential in hollow helicoid formation.<sup>[11]</sup> Powder X-ray diffraction (PXRD) patterns in Figure 1 clearly define as-synthesized and calcined

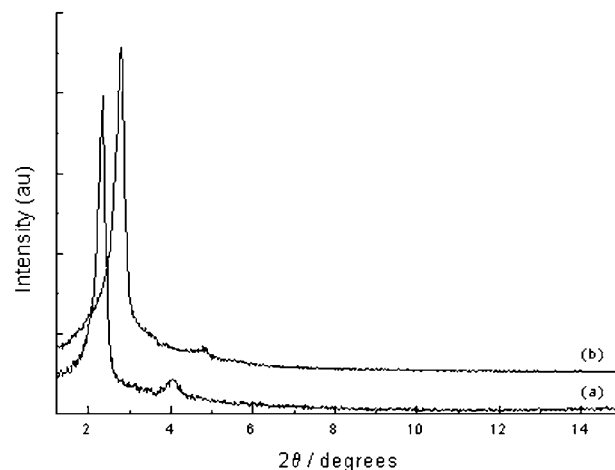


Fig. 1. Representative PXRD pattern for the a) as-synthesized and b) calcined hollow mesoporous silica morphologies.

materials as the MCM-41 hexagonal mesoporous silica.<sup>[12]</sup> Scanning electron microscopy (SEM) images reveal morphologies consisting of extraordinary hollow helicoid shapes that resemble a screw thread, Figure 2a–c. Transmission electron microscopy (TEM) images, Figure 3a, on whole-mounted helicoids reveal that they are hollow with an approximately 1 μm thick “shell”. They are composed of hexagonally close-packed ca. 5 nm diameter channels which have an ca. 1 nm silica wall and appear to spiral around the major axis of the helicoid.

The dimensions of a collection of hollow helicoids have been analyzed by measurements of SEM images. It is striking that diagnostic dimensions of the screw, namely pitch width and angle, flute width, and inside and outside diameter, are found to span a rather narrow range. Notably, the pitch angles center around 70° and 110°, which correspond

[\*] Prof. G. A. Ozin, Dr. S. M. Yang, Dr. I. Sokolov, Dr. N. Coombs  
Materials Chemistry Research Group  
Lash Miller Chemical Laboratories  
University of Toronto  
80 St. George Street, Ontario M5S 3H6 (Canada)  
Dr. C. T. Kresge  
Mobil Technology Company  
Strategic Research Center  
Paulsboro, NJ 08066-0480 (USA)

[\*\*] GAO is deeply indebted to the Canada Council for the award of an Isaac Walton Killam Foundation Research Fellowship (1995–97). SMY is grateful to the Croucher Foundation, Hong Kong, for the award of a PDF in support of his research while at the University of Toronto. Financial support of this work from Mobil Technology Company is deeply appreciated.

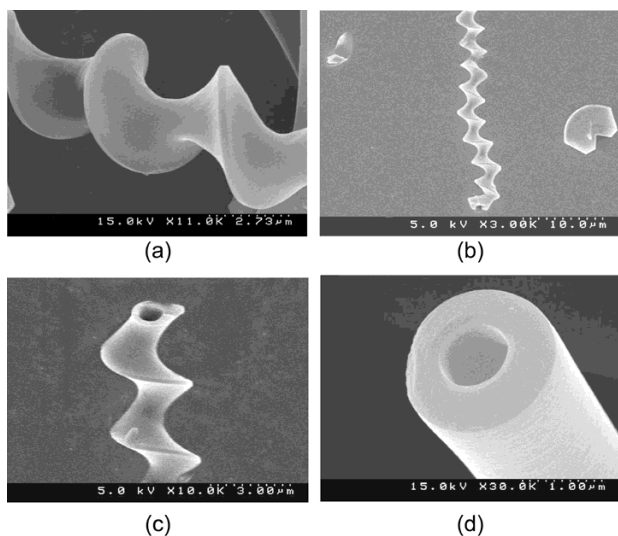


Fig. 2. SEM images of synthetic hexagonal mesoporous silica: a–c) hollow helicoids and d) hollow cylinder.

respectively to left- and right-handed helices that occur in essentially equal numbers within the same synthesis batch, Figure 4.

In developing a model for the morphogenesis of mesoporous silica hollow helicoids we note that in a synthesis, continuous mesoporous silica films were not found at the air–water interface. In addition to the hollow helicoid shapes, the synthesis also produces a significant yield of mesoporous silica open-ended hollow cylinders. SEM and

TEM images of whole mounted specimens define well-ordered channels whirling concentrically around the axis of the hollow cylinder (Fig. 2d and 3b). One can also observe the co-existence of folded sheets, helical ribbons, and incomplete tubes. All are comprised of the same hexagonal mesoporous silica material. This can be shown in a selected area electron diffraction (SAED) image, which defines the relation between the hexagonal channel structure and morphology of a folded sheet (Fig. 5). From the collective evidence we conclude that helical hollow cylinders originate from polymerization-induced differential contraction of a patch of silicate liquid-crystal film formed at the air–water interface (Fig. 6a) and then into hollow helicoids of mesoporous silica (Fig. 6b and c).

To expand, the folding mechanism emerges from both radial and longitudinal contractions across and parallel to the rods/channels respectively, both of which are induced by polymerization of silicate to silica. As the patch grows in area and thickness, older rods must undergo more polymerization and contraction than the younger ones. Provided we consider radial and longitudinal differential contractions in thickness, they lead to diagonal bending of the patch because these two contractions act in mutually orthogonal directions. For an energetically favorable configuration, the volume of the micelle rods within the diagonally folded patch changes solely by contraction and not deformation. Therefore, the folded patch is considered to be stress-free. Parameters for such a configuration emerge from a purely geometrical approach and turn out to be a

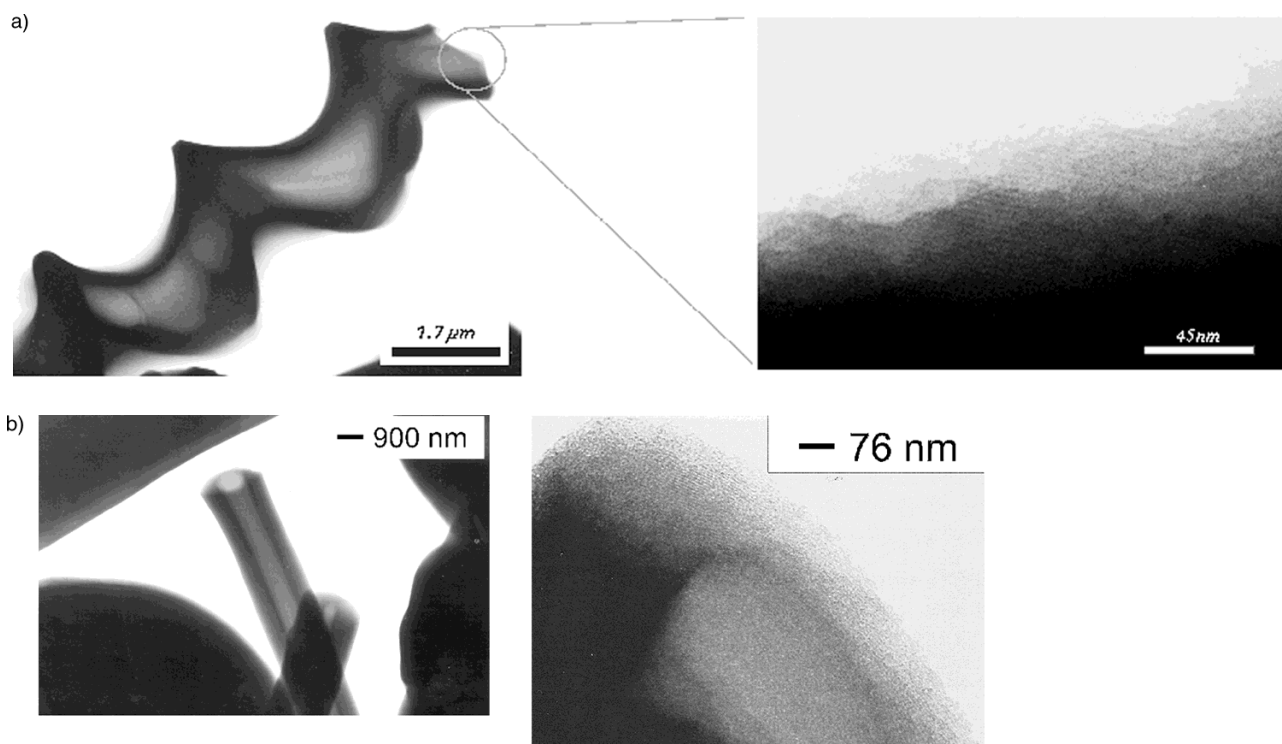


Fig. 3. TEM images of whole mounted synthetic hexagonal mesoporous silica a) hollow helicoids (right) with a shell composed of ca. 50 Å mesoporous channels, which follow the generating curve of the helicoid (left), b) hollow cylinders (left) with wall comprised of ca. 50 Å mesoporous channels, which whirl concentrically around the main axis of the cylinder (right).

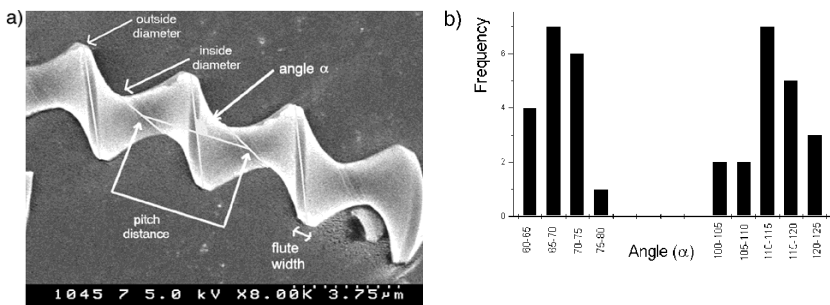


Fig. 4. Histogram of the distribution of mesoporous silica hollow helicoid parameters a) characteristic dimensions and b) pitch angle (right-handed for  $\alpha < 90^\circ$  and left-handed for  $\alpha > 90^\circ$ ). The pitch angles ( $\alpha$ ) were measured according to (a) from 37 SEM images with a magnification from 5 k to 10 k.

cylinder (Fig. 6a) in which the micellar rods are pitched with a constant angle,  $\alpha$ , relative to the principal axis:

$$\alpha = \arctan \frac{1-\bar{\gamma}_L}{1-\bar{\gamma}_R} \bar{\gamma}_R \equiv \frac{\gamma_R(R_{in})}{\gamma_R(R_{out})}, \bar{\gamma}_L \equiv \frac{\gamma_L(R_{in})}{\gamma_L(R_{out})} \quad (1)$$

where  $\gamma_L$  and  $\gamma_R$  are longitudinal and radial contraction factors and  $R_{in}$ ,  $R_{out}$  are internal and external radii of the resultant cylinder, respectively.

The contraction factor  $\gamma_R$  has been obtained from X-ray diffraction data which provides the rod center-to-center distance before and after polymerization; it is estimated to be in the range from 0.6 to 1.  $\gamma_L$  is obtained from the contraction expected for the condensation process  $\text{SiOH} + \text{HOSi} \rightarrow \text{SiOSi}$ ; it is estimated to be around 0.6 for complete polymerization.<sup>[13]</sup>

To understand the case of both orthogonal and parallel differential contractions with respect to the surface of the patch, it is convenient to artificially separate the effect of bending due to polymerization in these two directions. This is possible because the configuration is free of internal stresses (see above) and therefore one stage is unlikely to influence the other. Orthogonal differential contraction gives the aforementioned hollow helical cylinder, Figure 6a is constructed from a set of  $N$  rods and described by the following set of equations, where  $i = 1, 2, 3$ ;  $N$  is the rod number and  $d$  is the rod diameter:

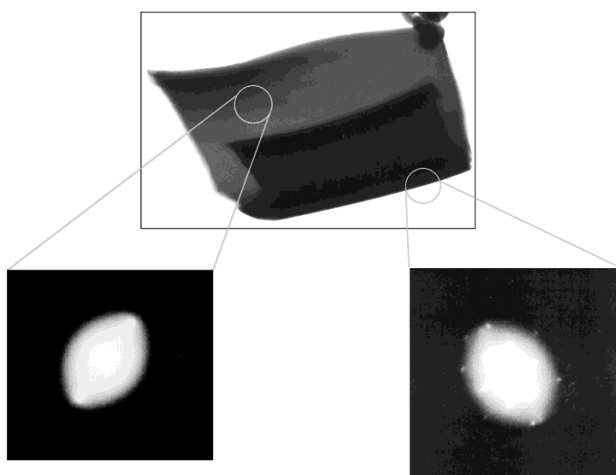


Fig. 5. Selected area electron diffraction (SAED) patterns of a folded sheet shows a hexagonal symmetry end-on channel pattern (001) in the curling region (right) and the linear side-on channel pattern (2T0) in the flat region (left).

$$z_i = \left( \varphi + \sum_{k=1}^i \frac{d}{\rho \cos \alpha} \right) \frac{\rho}{\tan \alpha} = \frac{\rho \varphi}{\tan \alpha} + \frac{id}{\sin \alpha} \quad (2)$$

Consider next differential contraction parallel to the surface of the cylinder. If we consider an infinite cylinder in which the contraction is independent of the position on the rod, then each point on the rod experiences the same tension in opposite directions. Therefore only rearrangements perpendicular to the rods, in the radial direction of the cylinder can occur. From this one can derive that  $\rho_i/\tan \alpha_i$  is independent of  $i$  where  $\rho_i$  and  $\alpha_i$  are the helicoid radius and angle of the  $i$ th rod just after beginning the second stage. From the geometry of the hollow helical cylinder the radius of the  $i$ th rod must change according to  $\rho_i \rightarrow \gamma_{Ti} \rho$ . Taking all of these into account one can obtain the equation of the contracted hollow tube:

$$x_i = \gamma_{Li} \rho \cos \varphi, y_i = \gamma_{Li} \rho \sin \varphi$$

$$z_i = \left( \varphi + \sum_{k=1}^i \frac{d}{\gamma_{Li} \rho \cos \alpha} \right) \frac{\rho}{\tan \alpha} \quad (3)$$

Examples of this simulation are shown in Figure 6b and c. One can see an obvious resemblance to the experimental images.

It should be noted that the laws describing the transformation of both  $r$  and  $\alpha$  are fixed by the extent of polymerization-induced contraction of silicate to silica. From the conservation of  $N$  channels during contraction, and Equation 2, one can write:

$$\frac{d}{\rho} \sum_{i=1}^N \sqrt{\tan^2 \alpha + \frac{1}{\gamma_{Li}^2}} = 2\pi \quad (4)$$

Qualitatively however, the validity of this equation breaks down due to the dependence of  $\rho_{Li}$  on  $i$ , and the deviation of  $\gamma_{Li}$  from unity. Nevertheless, if  $\tan \alpha > 1/\gamma_{Li}$  then  $\gamma_{Li}$  does not significantly influence the value of the left-hand side of Equation 4 and so it is approximately valid. In other words, for  $\alpha > 60^\circ$  ( $\gamma_{Li} \sim 0.6$ ), we can use the geometrical approach to rationalize the morphogenesis of hollow helicoid shapes otherwise internal stresses will occur in the helicoid, which should make its formation energetically unfavorable. This restriction on the angle  $\alpha$  is in good agreement with the observed lower limit of  $60^\circ$  for the pitch angle. The upper limit of ca.  $80^\circ$  can also be accommodated by the model.

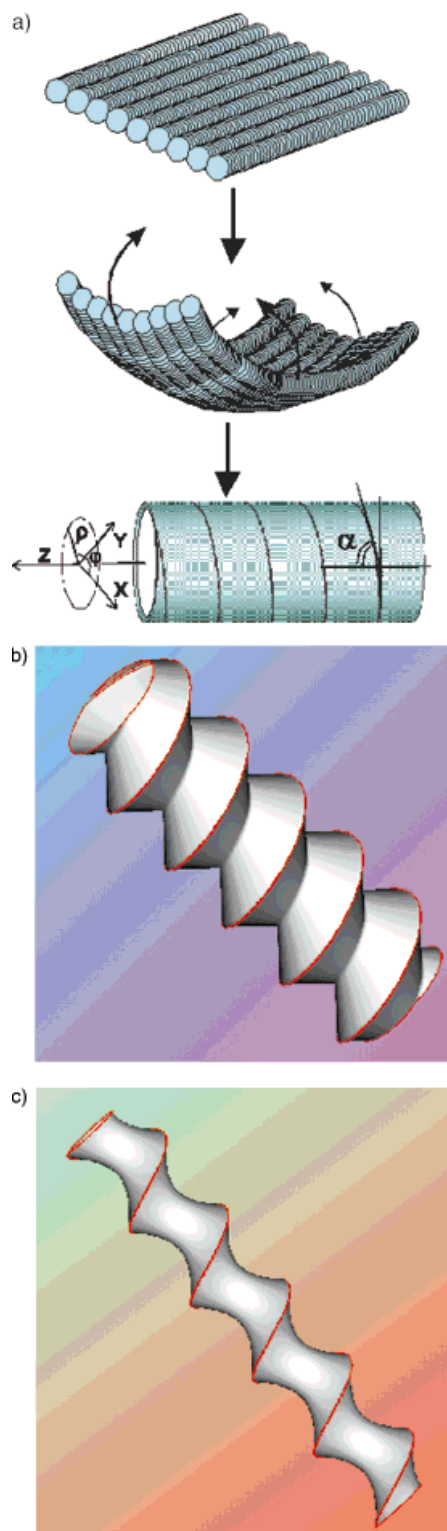


Fig. 6. a) Supramolecular Origami folding model of a patch of polymerizable hexagonal silicate liquid crystal that creates a helical hollow cylinder of silicate micellar rods or silica channels coiling around the main axis. The highlighted black solid line represents a single rod or channel and  $\alpha$  denotes the pitch angle of the helix. A simulation of the morphogenesis of hollow helicoids of mesoporous silica by polymerization-induced differential contraction of a helical hollow cylindrical silicate mesophase, b) linear contraction  $\gamma_{Lz} = 0.5$  to 1,  $\alpha = 80^\circ$ , and c) quadratic contraction,  $\gamma_{Lz} = 0.5$  to 1,  $\alpha = 70^\circ$ . The channels follow the generating curve of the helix.

It is important to note that the “hollow helicoids” made of mesoporous silica and described for the first time in this paper, have the shape of an “Archimedean screw”. They are morphologically distinct to mesoporous silica “shell mimics” grown in solution<sup>[14]</sup> and topologically different to mesoporous silica “spiral fiber” grown at the interface between oil and water.<sup>[9]</sup>

In conclusion, a self-organizing synthesis involving a new kind of growth mechanism has been described that reproducibly produces novel hollow helicoid morphologies made up of hexagonal mesoporous silica. The understanding that has emerged from this study may reveal new ways of controlling the growth and form of composite inorganic–organic mesostructured materials with unique topologies, functions, and applications. Siliceous hollow helicoids with spiraling mesoscale channels may find application in separating viral or bacterial particles, chiral catalysis of macromolecules, and micromolds for the fabrication of magnetically activated screws in micromechanical, microfluidic, and microanalytical devices. The ability to intentionally synthesize micrometer-sized shaped objects, such as mesoporous silica fibers, discs, gyroids, toroids, spheres, hollow cylinders, and hollow helicoids<sup>[10,14,15]</sup> begins to point the way to the idea of self-assembling “synthetic” microelectromechanical machines (SMEMS) as an alternative or adjunct to the currently employed MEMS techniques, which rely on the fabrication of components.<sup>[16]</sup> This paradigm of “shape assembly” raises some intriguing possibilities for future research aimed at the organization and integration of synthetically shaped materials for functional devices.<sup>[16]</sup>

## Experimental

**Materials:** Tetraethylorthosilicate (TEOS, 99.99%, Aldrich), cetyltrimethylammonium chloride (CTACl, 29 wt.-% aqueous solution, Pflatz & Bauer), formamide (99%, Aldrich) and hydrochloric acid (36.5–38 wt.-% aqueous solution, BDH) were used as received.

**Synthesis:** A mixture of H<sub>2</sub>O/CTACl/HCl/formamide was stirred in a polypropylene bottle at room temperature for 2 days, after which TEOS was added and the solution stirred for ca. 5 min. The solution was then kept under quiescent conditions for 3 days. The molar ratio of H<sub>2</sub>O:HCl:formamide:CTACl:TEOS was 100:7.8:9.4–10.2:0.11:0.13. The materials so formed were filtered, washed with copious amounts of water, and air-dried.

**Characterization:** Scanning electron microscopy (SEM) images were carried out on a Hitachi S-4500 field emission microscope. The samples were covered with a thin layer of gold to prevent any charging. Transmission electron microscopy (TEM) images and the Selected area electron diffraction (SAED) pattern were recorded on a Philips 430 microscope operating at 100 kV. The samples were dispersed in ethanol, placed onto a copper grid and then air-dried.

Received: May 31, 1999  
Final version: August 16, 1999

- [1] B. Deppert-Lippitz, *Die Schraube zwischen Macht und Pracht: das Gewinde in der Antike*, Sigmaringen, Thorbecke **1995**.
- [2] J. R. Winkler, H. B. Gray, *Acc. Chem. Res.* **1998**, *31*, 698.
- [3] B. I. Yokobson, R. E. Smalley, *Am. Sci.* **1997**, *85*, 324.
- [4] J. W. Mintmire, C. T. White, *Carbon* **1995**, *33*, 893.
- [5] J. M. Garcia-Ruiz, *J. Cryst. Growth* **1985**, *73*, 251.
- [6] S. Mann, *J. Chem. Soc., Dalton Trans.* **1997**, *21*, 3953.
- [7] J. D. Hopwood, S. Mann, *Chem. Mater.* **1997**, *9*, 1819.
- [8] L. A. Gower, D. A. Tirrell, *J. Cryst. Growth* **1998**, *191*, 153.

- [9] Q. Huo, D. Zhao, J. Feng, K. Weston, S. K. Buratto, G. D. Stucky, S. Schacht, F. Schüth, *Adv. Mater.* **1997**, *9*, 974.  
 [10] H. Yang, N. Coombs, G. A. Ozin, *Nature* **1997**, *386*, 692.  
 [11] H. Yang, N. Coombs, I. Sokolov, G. A. Ozin, *Nature* **1996**, *381*, 589.  
 [12] C. T. Kresge, M. Leonowicz, W. J. Roth, J. C. Vartuli, J. C. Beck, *Nature* **1992**, *359*, 710.  
 [13] A. Firouzi, D. J. Schaefer, S. H. Tolbert, G. D. Stucky, B. F. Chmelka, *J. Am. Chem. Soc.* **1997**, *119*, 9466.  
 [14] G. A. Ozin, H. Yang, I. Sokolov, N. Coombs, *Adv. Mater.* **1997**, *9*, 662.  
 [15] H. Yang, G. Vovk, N. Coombs, I. Sokolov, G. A. Ozin, *J. Mater. Chem.* **1998**, *8*, 743.  
 [16] H. L. Tuller, R. Mlcak, *Curr. Opin. Solid State Mater. Sci.* **1998**, *3*, 501.

## Patterning Self-Assembled Monolayers on Oxide Surfaces Using a Lift-off Technique\*\*

By Stefan Walheim, Rainer Müller, Monika Sprenger, Edgar Loser, Jürgen Mlynek, and Ullrich Steiner\*

Since its discovery six years ago,<sup>[1]</sup> microcontact printing of self-assembled monolayers (SAMs) on Au surfaces has gained remarkable popularity, mainly due to the ease of its application, compared to other lithographic techniques.<sup>[2]</sup> The pattern formation technique of  $\mu$ CP is modeled in close analogy to macroscopic relief printing. A master with a topographic pattern is used to cast an elastomeric stamp. Stamping an ink onto a surface reproduces the pattern of the master. Most commonly, the ink is a solution of thiol-terminated alkane chains in ethanol, which react with the substrate surface to form a SAM. Lateral structure-sizes down to 100 nm have been reported.<sup>[3,4]</sup> Unfortunately, the use of the thiol end-group restricts the choice of surfaces to Au, Ag, and Cu.<sup>[2]</sup>

For many experiments in physics, chemistry, and biology, as well as for certain technological applications, the extension of  $\mu$ CP to other substrate materials is desirable, in particular when transparent or non-conducting surfaces are required. Alkane molecules with various anchor groups such as alkane-silanes have been employed to generate SAMs on oxide surfaces.  $\mu$ CP using these molecules has recently been reported.<sup>[5-7]</sup> It is, however, unlikely that this technique will gain the popularity that  $\mu$ CP of alkane-thiols enjoys today. The main difference between the chemisorption of thiols on gold and the silane reaction is the role of the water. H<sub>2</sub>O is an essential ingredient in the silane reaction. The perfection of silane-based SAMs sensitively de-

pends on the H<sub>2</sub>O content in the solvent and the amount of adsorbed water on the substrate. This makes the results of  $\mu$ CP of silanes strongly dependent on environmental parameters such as humidity and temperature.

In this letter, we report a lift-off technique, which extends the ease and reproducibility of  $\mu$ CP of alkane-thiols on Au to virtually any surface onto which SAMs can be grafted. To circumvent the problems caused by the water sensitivity of the silane reaction, we make use of the more robust thiol chemistry (first row, Fig. 1). First, a 10 nm thick Au film is evaporated onto a silicon oxide surface. To guarantee sufficient adhesion of the Au to the substrate, a thin (<2 nm) Ti layer is deposited prior to the evaporation of the Au. A rubber stamp (Sylgard 184, Dow Corning) is soaked in an octadecylthiol (ODT) solution (1 mmol in ethanol) and pressed onto the Au surface. This results in a patterned SAM of ODT (Fig. 1a). The gold regions that are not protected by the SAM are etched away by a cyanide solution (1 mmol potassium thiosulfate, 0.1 mmol potassium ferricyanide, 0.01 mmol potassium hexacyanoferrate(II)trihydrate, 10 mmol potassium hydroxide in H<sub>2</sub>O for 10 min). After cleaning the surface using a "snow-jet"<sup>[8]</sup> (Fig. 1b), the sample is subjected for ~1 h to an octadecylsilane (OTS) solution (0.25 % in hexane), which forms a SAM on the now exposed oxide surface (Fig. 1c). In a last step, a bromine-methanol etching solution (1:80, 30 s) followed by a snow-jet treatment removes the remaining Au, revealing a laterally patterned oxide surface (Fig. 1d). In our present experiment, the contribution of the thin Ti layer is not completely understood. While it is unlikely that the Ti is removed by the two etching steps, we expect it to completely oxidize in the etching solution. For most applications, we expect the presence of a thin titanium oxide surface to be of no consequence. Future X-ray photoelectron spectroscopy (XPS) measurements should resolve this issue.

The perfect replication of a stamped ODT pattern to an inverted OTS structure is demonstrated in Figure 1. The second row in Figure 1 shows topography images taken with an atomic force microscope (AFM) in contact mode, using a silicon tip, which was rendered unpolar by an OTS layer. The third row shows images that result from a lateral variation of the friction coefficient, yielding a lateral material contrast. We have chosen a 16 × 16  $\mu$ m scan area which includes the edge of a stamped stripe pattern. While the stamped lines are very regular in the interior part of the stamp (Fig. 2), the irregularities at the stamp edges serve to illustrate the precision of our technique. In Figure 1a, the bright surface regions are ODT covered, leaving darker 1–2 nm deep grooves of the bare Au substrate. This is reflected in the friction image, where the ODT features a lower friction coefficient (dark) compared to the Au (bright). After the first etching step (Fig. 1b) the contrast in the topography has increased, revealing the thickness of the Au film (~10 nm). The friction image is comparable to Figure 1a, due to similar friction coefficients of the Au and oxide surfaces. After deposition of the OTS layer (Fig. 1c),

[\*] Prof. U. Steiner,<sup>[+]</sup> S. Walheim, R. Müller, M. Sprenger, E. Loser, Prof. J. Mlynek  
Fakultät für Physik, Universität Konstanz  
D-78457 Konstanz (Germany)

[+] Second address: Department of Polymer Chemistry, University of Groningen, Nijenborgh 4, NL-9747 AG Groningen, The Netherlands.

[\*\*] We are grateful to Dr. Zulehner and Wacker-Chemie GmbH for supplying the silicon wafers. The help of Erik Schäffer with the manuscript is gratefully acknowledged. This work was funded by the Deutsche Forschungsgemeinschaft (DFG) (Sonderforschungsbereich 513, B2 and Schwerpunktprogramm "Benutzung und Strukturbildung an Grenzflächen") and the State of Baden-Württemberg (Optikzentrum Konstanz). US acknowledges receiving a Heisenberg fellowship by the DFG.